applied sciences

MDPI

Article

Rapid Estimation of Moisture Content in Unpeeled Potato Tubers Using Hyperspectral Imaging

Priyanga Muruganantham [1,*], Nahidul Hoque Samrat [1], Nahina Islam [1], Joel Johnson [2], Santoso Wibowo [1] and Srimannarayana Grandhi [1]

[1] School of Engineering and Technology, Central Queensland University, Melbourne 3000, Australia
[2] School of Health, Medical and Applied Sciences, Central Queensland University, Rockhampton 4702, Australia
* Correspondence: p.muruganantham@cqumail.com

Abstract: Potato (*Solanum tuberosum* L.) is one of the most significant vegetable crops grown globally, especially in developing countries. Over the last few years, global potato production has been increasing. This growth has created many opportunities for developing a wide range of value-added products from these crops. However, this requires monitoring the quality components of the tubers, such as moisture content, starch content, and soluble solid content. In particular, moisture content is one of the key quality parameters important for ensuring quality control throughout the supply chain and processing for consumer consumption. Ideally, moisture content would be estimated at the field level; however, current methods used by the industry to assess moisture content are time-consuming, labor-intensive, and destructive. Hence, the purpose of this study is to investigate the feasibility of hyperspectral imaging to quantify the moisture content of unpeeled potatoes before they were subsequently stored and processed. Hyperspectral images are collected from 47 intact potato tubers, with partial least squares regression (PLSR) models developed to predict moisture content from these spectra. The models showed predictive abilities for moisture content with acceptable ratios of prediction to deviation (RPDs) when considering the complete wavelength range (R^2 = 0.53, RPD = 1.46, root mean square error (RMSE) = 5.04%) or the β-coefficient wavelength selection technique (R^2 = 0.53, RPD = 1.47, RMSE = 5.02%). Furthermore, the prediction ability increased by more than 10% when the model wavelength was narrowed down to 733–970 nm. This study demonstrates the potential of using hyperspectral imaging for the quality assessment of intact, unpeeled potatoes, although further work is required to improve the model quality and implement this approach using remote sensing imagery.

Keywords: moisture content; potato; hyperspectral imaging; infield assessment; post-harvest handling

check for updates

Citation: Muruganantham, P.; Samrat, N.H.; Islam, N.; Johnson, J.; Wibowo, S.; Grandhi, S. Rapid Estimation of Moisture Content in Unpeeled Potato Tubers Using Hyperspectral Imaging. *Appl. Sci.* **2023**, *13*, 53. https://doi.org/10.3390/app13010053

Academic Editor: António José Madeira Nogueira

Received: 28 November 2022
Revised: 15 December 2022
Accepted: 16 December 2022
Published: 21 December 2022

Copyright: © 2022 by the authors. Licensee MDPI, Basel, Switzerland. This article is an open access article distributed under the terms and conditions of the Creative Commons Attribution (CC BY) license (https://creativecommons.org/licenses/by/4.0/).

1. Introduction

Potato is an important vegetable-tuber crop that is considered an integral part of food production systems across the globe. It is a key staple food and is the world's topmost non-grain food product. It is the third most important food crop after rice and wheat in about 130 countries, of which around 95 are developing countries [1]. Even though global production levels have increased by 20% since 1990, around 32% of potatoes are lost every year due to the lack of proper management, storage, and/or processing [1,2].

Potatoes are a nutritious food containing high levels of carbohydrates (principally in the form of starch), as well as protein, essential amino acids, potassium, and vitamin C, all of which are necessary nutrients for the human body [3]. Potatoes are widely consumed boiled, fried, or mashed, or they may be processed into chips, French fries, granules, flakes, flour, and other products. The quality, color, and appearance of the potato slices play a major role in the production and acceptability of consumers. Consequently, the quality of the potatoes used for processing purposes is essential for producing high-quality value-added products; however, rapid, cost-effective quality assessment remains challenging. In

potato processing, the preprocessing moisture content is one of the most critical parameters. Moisture content is an important factor in potatoes because it influences the quality of the product during the drying method in potato processing, and it is also associated with the rate of shrinkage and color of the potato [4,5]. Excessive moisture content can also lead to product spoilage as it aids the growth and activities of microorganisms [6]. Moreover, the freshness of freshly cut potato slices is related to their moisture content. Hence, knowledge about the moisture content of potatoes can assist in effectively preserving product quality and preventing spoilage.

Moisture content is traditionally determined using standard drying methods involving human inspection, oven-drying, and freeze-drying. However, these methods are not highly accurate, time- and energy-consuming, interruptive, and destructive [7]. Recent advancements in technology have made it possible to develop methods to determine moisture content utilizing imaging techniques. One of the rapid, convenient, and nondestructive approaches to measure moisture content is by using near-infrared spectroscopy. Despite this advancement in technology, these measurements are only taken from a single point, these techniques are unable to predict the moisture distribution [8], and cannot give information on the spatial distribution of moisture in the samples [9,10].

RGB and near-infrared spectroscopy (NIR) sensors have shown to be effective in a variety of agriculture and its related applications. However, it is found that only hyperspectral sensors have the spectral resolution that surpasses the use of multispectral imaging [11–13]. Several studies [14–16] have indicated that hyperspectral imaging (HSI) can be efficiently used in a variety of agriculture and related applications. Tahmasbian et al. [15] compared the effectiveness of HSI and NIRS in determining nitrogen and carbon concentrations in wheat. The authors stated that the scanning technology of HSI is more accurate than NIRS. The authors added that HSI can scan thousands to millions of pixels within an image compared to NIRS, which scans just one point. Due to the fact that they extract spectra sets made up of hundreds of bands across pictures with high spatial resolution, hyperspectral sensors typically produce enormous volumes of data [14]. Remote sensing, especially unmanned aerial vehicle combined with an HSI sensor, is used in various areas, such as observing crop cultivation stages, estimation of parameters (e.g., carotenoid content, moisture content, and biomass), and disease monitoring, as they have a wider spectral range and narrow bands. Mozgeris et al. [16] predicted the chlorophyll concentration and NDRE of spring wheat using Rikola hyperspectral HSI with UAV, which outperformed color infrared (CIR) imagery. Aasen et al. [17,18] measured the chlorophyll of barley using a snapshot hyperspectral camera on a UAV.

HSI is an analytical technique combining the benefit of spectroscopy and digital imaging for obtaining both spectral information of samples in the visible region and near-infrared region and spatial information. HSI has been used in agriculture for determining product quality, including physical, chemical, and biological attributes. As with near-infrared spectroscopy, this technique is rapid, nondestructive, and efficient. HSI is simple to handle, which helps in processing and analyzing the data and acquiring important information required to establish the correlation between desired quality parameters and hyperspectral image data. There have been numerous previous applications of HSI in determining the quality of agricultural produce, such as: estimation of moisture content in banana [19], glucose estimation in carrot and banana [20,21], estimation of moisture content, firmness and pH values in apple [7], and prediction of moisture content in peanut [22]. In the case of potatoes, studies investigating quality assessment using HSI include estimation of moisture content with and without skin [23], starch, soluble sugars and amino acids estimation [24], estimation of starch content [25], evaluating sugar content [26], biomass estimation [27], detection of nitrogen stress [28], nondestructive detection of blackspot [29], classification of bruised potato [30], precautionary analysis of sprouting potato eyes [31], prediction of soluble solid content in sweet potato [32], determination of moisture content and chromacity during convective hot air drying process [4], prediction of optimal cooking time for boiled potatoes [33], detecting water stress in potatoes [34], prediction of moisture content and

freezable water content of purple-fleshed sweet potato slices [35], and prediction of color and water content of fresh cut potato slices [36]. However, there are limited studies using HSI and machine learning algorithm for the estimation of moisture content in potatoes.

Therefore, this study demonstrates the potential use of HSI using machine learning for estimating the moisture content of unpeeled whole potato tubers. The ultimate aim would be to implement the HSI technique for infield operations using remote sensing sensors to reduce post-harvest loss of potato tubers.

2. Materials and Methods

2.1. Sample Collection and Analysis

For scanning the unpeeled potato samples, a Specim IQ hyperspectral VS_NIR camera (Specim, Spectral Imaging Ltd., Oulu, Finland) was used with two 750 W tungsten halogen lamps (ARRILITE 750 Plus, ARRI, München, Germany) and a white reference tile. The Specim IQ hyperspectral VS-NIR camera was positioned with two symmetrically placed halogen lamps, and the white reference tile was properly positioned with the camera, as shown in Figure 1. Reflectance geometry is employed by the camera, which works between the range of 400 and 1000 nm, with a spectral resolution of −7 nm, thereby providing 204 wavebands. Accordingly, each hyperspectral image is a volumetric image cube that is a three-dimensional matrix storing spatial as well as spectral information about the sample.

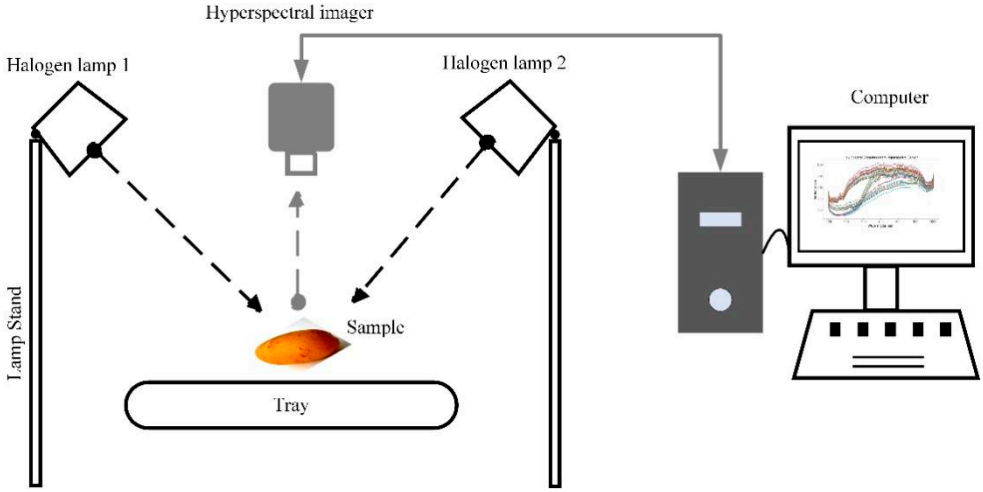


Figure 1. Hyperspectral imaging system in the laboratory.

A total of 47 samples of commercial different variety potatoes were collected from the local supermarkets around Central Queensland, Australia. The whole unpeeled potatoes in dry basis were used in the study. Before conducting the moisture analysis in the unpeeled potatoes, they were kept in a lab oven at 60 °C for two days. The ground truth moisture content was obtained by measuring the difference in potato weights before keeping the potatoes inside the oven, and, after, taking the potatoes that were left inside the oven at 60 °C for two days for drying. By presuming that moisture alone has been driven off after drying, the gravimetric microwave drying method estimates moisture indirectly [37]. The pretreatment was carried out to contain the moisture content in the potatoes. The moisture content of unpeeled potatoes varied between 50 and 80%, as shown in Figure 2.

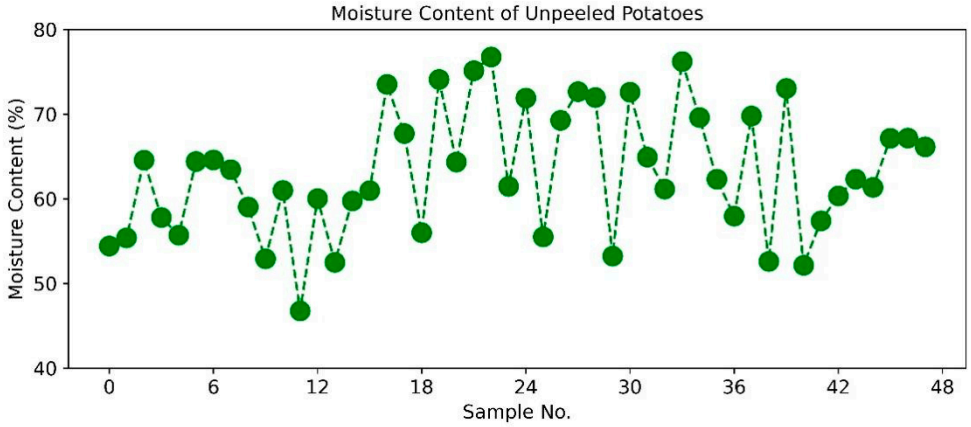


Figure 2. Moisture content of unpeeled potatoes.

2.2. Preprocessing

The hyperspectral datacube had a number of undesirable effects and noises, such as baseline shifts, light scattering, unrestrained external factor, and random noises that may influence the results. Prior to the development of multivariate models, spectral preprocessing was used to reduce unwanted effects and noises. An average spectrum was found by calculating the average spectrum from all pixels within the region of interest (ROI). This method was employed to smooth the impact of random noises across the region, and then it was used for further processing. The hyperspectral images were calibrated with a white and black reference image for removing the camera sensor's dark current influence [38]. By establishing a square region on ROI over the sample, the calibrated pictures were cropped. We conducted preprocessing based on methods previously mentioned in the literature [39–42].

2.3. Partial Least Squares Regression

Partial least squares regression (PLSR) was selected as a regression technique because of its high performance and the fact that it has been widely used for the analysis of HSI data from numerous crops [42–48]. PLSR enables us to investigate the relationship between multiple dependent and independent variables. In spectral data analysis, it has proven to be a dependable, resilient, and accurate method [47–49].

Based on the proposed PLSR model, the moisture content of the unpeeled potatoes was predicted from the respective HSI spectra (204 wavelengths). Prior to model creation, the dataset was randomly partitioned into training (80%) and test (20%) sets. The 'train test split' function from the sklearn.model selection python package was used to split the data into training and testing sets, with a value of 20 for the 'random state' parameter in the train test split function. To gain the optimum performance and avoid overfitting, the full cross-validation (leave-one-out) method was employed to calculate the number of latent variables (LVs) [50–52]. For determining the optimum number of LVs, initially, the root mean square error (RMSE) was calculated from the cross-validation set, and then the optimal number was selected from the minimum RMSE.

2.4. Model Evaluation

The evaluation metrics are used to validate a model based on accuracy or error rate, whereas some evaluation metrics are used as an analyzer for model selection or used as a discriminator to differentiate and choose the best model [53]. The evaluation metrics R^2 and RMSE of the training and testing datasets are used to assess a generated model's prediction abilities [46,54,55]. Meanwhile, the relative performance to deviation (RPD) is used to examine the predictability of the results [46,50,56]. According to Iqbal et al. [56] and John et al. [57], a model's predictive performance is regarded as 'excellent' when the RPD

value exceeds 1.4 and 'poor' when the RPD value is less than 1.4. The following equations are used to determine the R^2, RMSE, and RPD:

$$R^2 = \frac{\Sigma\left(y_{i,p} - y_{i,m}\right)^2}{\Sigma\left(y_{i,p} - \overline{y}\right)^2}$$

$$RMSE = \sqrt{\frac{1}{m}\sum_{i=m}^{m}\left(y_{i,p} - y_{i,m}\right)^2}$$

$$RPD = \frac{SD}{RMSE}$$

where y_p represents the predicted value, y_m represents the main value for the ith sample, m represents the number of samples, $\overline{y}$ is the average of the true loads of m samples, and SD represents the standard deviation of the predicted values in the training (T) and testing (V) sets. Figure 3 depicts a schematic representation of the complete data processing, analysis, and model generation process.

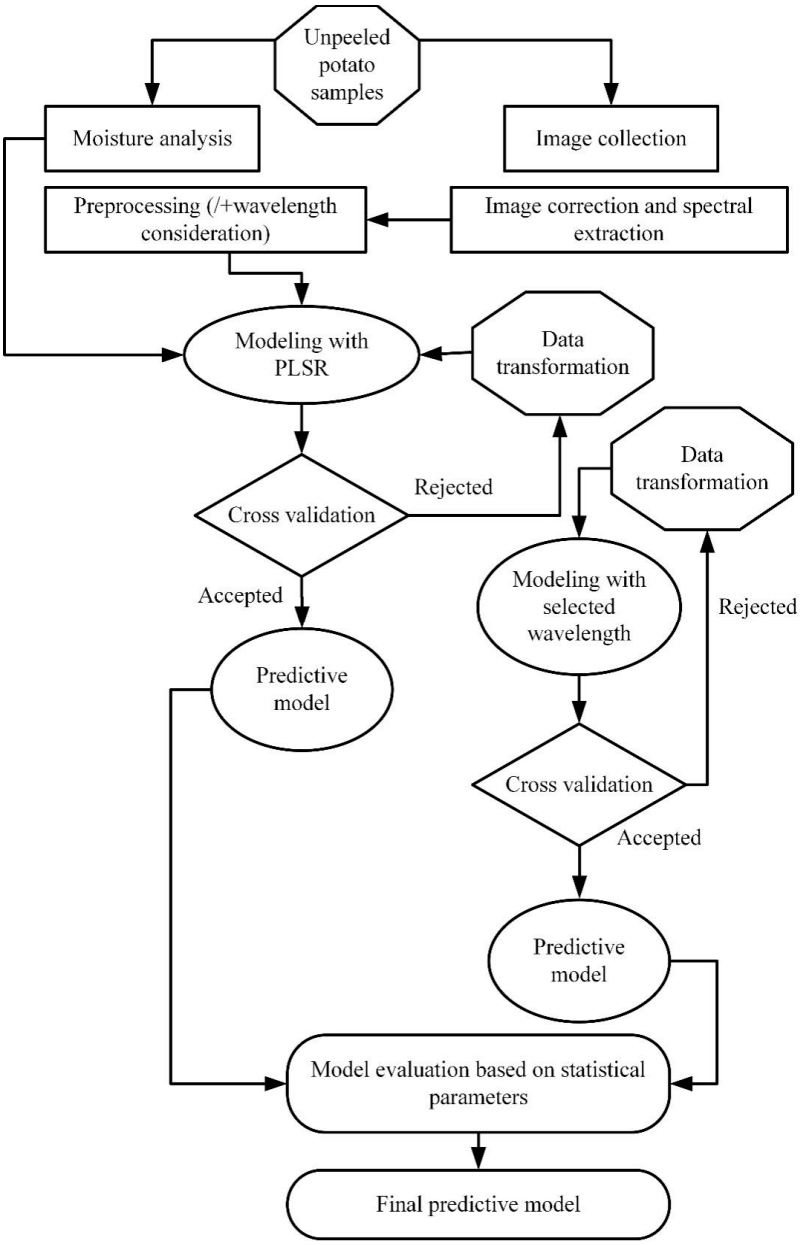


Figure 3. Schematic workflow of data processing.

The variable importance in the projection (VIP) and the PLSR regression coefficients, often known as β-coefficients, are frequently employed methods for choosing variables. In this paper, the PLSR regression β-coefficients of each variable were used to choose significant wavelengths. The vector of regression coefficients (β) was considered as it is a single measure of the extent of correlation between each variable and the response [58]. Based on [42,59], the PLSR model makes use of wavelengths with significant positive or negative β-coefficients, as they are crucial and contain valuable information. Similarly, variables with low absolute values of this filter measure and wavelengths with β-coefficient less than the standard deviation of all β-coefficients were removed from the investigation [58].

VIP is another technique that is frequently utilized for determining effective spectral regions. The VIP technique identifies variables by first computing the VIP score, and then eliminates variables with VIP scores below a specific threshold [42,58]. On the basis of the suggestions from [42], the threshold value in this study was determined at 1.

3. Results and Discussion

Before preprocessing the spectrum data, the average spectrum of all the pixels inside the ROI of each unpeeled potato sample was computed. The averaged spectra were subjected to preprocessing techniques, such as standard normal variate (SNV), mean filter with 5 × 5 window size (MF5), mean filter with 9 × 9 window size (MF9), the first and second derivatives calculated using Savitzky–Golay smoothing (1D-SG and 2D-SG), and multiplicative scatter correction (MSC). The original averaged spectra and their related preprocessed spectra were used to create the PLSR model. A total of seven PLSR models were created based on the preprocessing procedures performed on the HSI dataset before determining the best wavelengths, where 204 spectral bands are recorded by the hyperspectral sensor at wavelengths ranging from 397.32 to 1003.58 nm [60]. Similarly, 79 spectral bands are recorded at wavelengths ranging from 732.53 to 969.63. The key statistical metrics utilized to evaluate the performance of the PLSR model including latent variables (LVs), R^2, RMSE, and RPD, are included in Tables 1 and 2 respectively.

Table 1. The PLSR results when considering the full HSI wavelengths between 397.32 and 1003.58 (a total of 204 spectral bands).

Model	Preprocessing Method	LV	Wavelength (A/B/C)	No Wavelength Selection			VIP Based Wavelength Selection			β-Coefficient Wavelength Selection		
				R^2	RPD	RMSE	R^2	RPD	RMSE	R^2	RPD	RMSE
I	NO	8	204/73/51	0.53	1.46	5.04	0.51	1.43	5.16	0.53	1.47	5.02
II	1D-SG	6	204/61/61	0.48	1.39	5.29	0.46	1.36	5.40	0.48	1.38	5.32
III	2D-SG	2	204/75/57	0.26	1.16	6.34	0.29	1.18	6.22	0.30	1.19	6.18
IV	SNV	7	204/65/52	0.45	1.35	5.46	0.40	1.29	5.73	0.43	1.33	5.54
V	MSC	7	204/62/51	0.47	1.37	5.36	0.44	1.34	5.50	0.47	1.37	5.36
VI	MF5	8	204/66/53	0.49	1.40	5.27	0.47	1.38	5.35	0.44	1.34	5.49
VII	MF9	8	204/67/56	0.47	1.38	5.35	0.45	1.35	5.44	0.41	1.30	5.66

The R^2 value between the predicted and measured moisture content was used to assess the prediction models' performance via RMSE and RPD, respectively. The model was considered good if RMSE was low and both R^2 and RPD were high. The PLSR results when considering full HSI wavelengths were compared with results when selecting important wavelength ranges. It was tested to see if choosing significant wavelengths increased the models' ability to predict outcomes more accurately. A total of seven models were developed using the β-coefficient and VIP wavelength selection methods. When full HSI wavelengths were considered, six of the seven models performed poorly (RPD < 1.4) and only the PLSR β-coefficient (R^2 = 0.53, RMSE = 5.02, and RPD = 1.47) and PLSR no

wavelength selection (R^2 = 0.53, RMSE = 5.04, and RPD = 1.46) with no preprocessing technique showed acceptable performance (RPD > 1.4). The performance based on VIP wavelength selection was low (R^2 = 0.51, RMSE = 5.16, and RPD = 1.43) when compared with no wavelength selection and β-coefficient wavelength selection. Figure 4 shows that the optimum model created using β-coefficient wavelength selection with no preprocessing also showed acceptable performance (R^2 = 0.53, RMSE = 5.02, and RPD = 1.47). It can also be observed that there is not much difference between the performance of Model I with no wavelength selection and with β-coefficient wavelength selection.

Table 2. The PLSR results when considering wavelengths between 732.53 and 969.63 nm (a total of 79 spectral bands).

Model	Preprocessing Method	LV	Wavelength (A/B/C)	No Wavelength Selection			VIP Based Wavelength Selection			β-Coefficient Wavelength Selection		
				R^2	RPD	RMSE	R^2	RPD	RMSE	R^2	RPD	RMSE
I	NO	2	79/17/13	0.07	1.04	7.11	0.07	1.03	7.12	0.07	1.03	7.12
II	1D-SG	12	79/28/27	0.66	1.71	4.31	0.58	1.55	4.77	0.64	1.67	4.40
III	2D-SG	1	79/46/46	0.10	1.05	7.00	0.10	1.05	7.01	0.10	1.05	7.01
IV	SNV	2	79/14/14	0.22	1.13	6.53	0.22	1.13	6.50	0.22	1.13	6.51
V	MSC	2	79/16/18	0.18	1.10	6.69	0.18	1.10	6.67	0.18	1.10	6.67
VI	MF5	2	79/17/14	0.07	1.04	7.11	0.07	1.03	7.12	0.07	1.03	7.12
VII	MF9	2	79/18/15	0.07	1.04	7.11	0.07	1.03	7.13	0.07	1.03	7.12

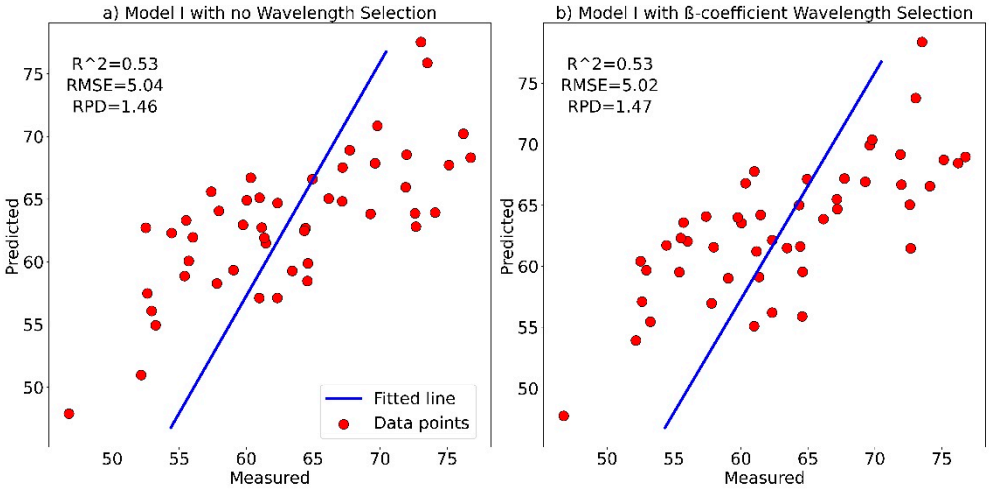


Figure 4. Measured vs. predicted moisture content in PLSR regression.

The selection of critical wavelengths was then carried out to see if this enhanced the models' prediction accuracy. Using the β-coefficient variable selection approach, the number of wavelengths in the PLSR models effectively decreased to 79 spectral bands, i.e., the wavelengths from 732.53 to 969.63 nm were considered, as shown in Figure 5. In this case, the performance of only one model (i.e., 1D-SG preprocessing) was acceptable (RPD $\geq$ 1.4) when considering both no wavelength selection and β-coefficient wavelength selection. Moreover, the 1D-SG preprocessing methodology performance for the reduced wavelength range was superior to the PLSR models utilizing the full wavelength range (R^2 = 0.66, RMSE = 4.31, and RPD $\geq$ 1.71). However, the selection of PLSR wavelengths through the β-coefficient method did not improve the accuracy of this model (R^2 = 0.64, RMSE = 4.40, and RPD = 1.67) as shown in Figure 6. Nevertheless, Table 1 shows that both models showed better performance using the reduced wavelength range compared to the models utilizing all wavelengths. The VIP-based wavelength selection performance

was comparatively low in both the cases when we considered full wavelength and when considering wavelengths between 732.53 and 969.63 nm. Based on Figures 5 and 6, it can be seen that model II with optimum wavelength (732.53–969.63 nm) selection performed well compared to model I with full wavelength selection.

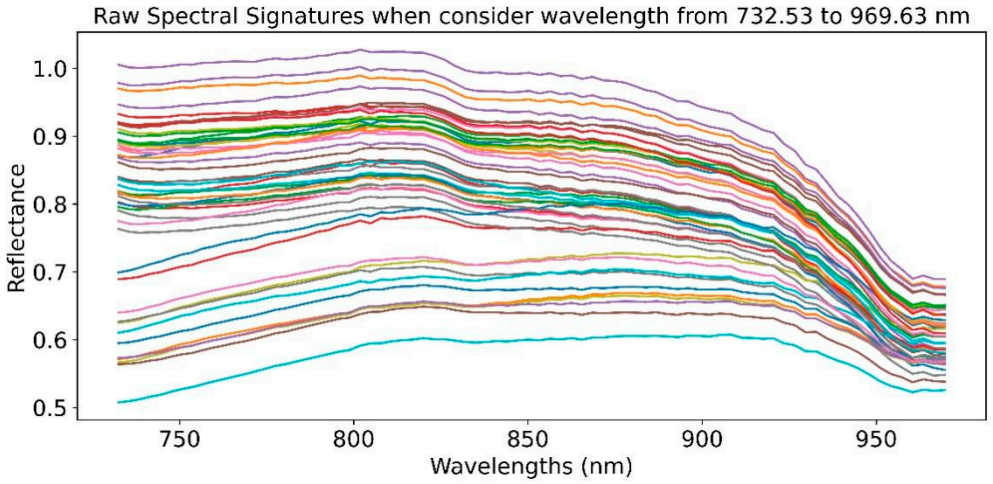


Figure 5. Raw spectral signatures when considering wavelength from 700 nm to 1000 nm.

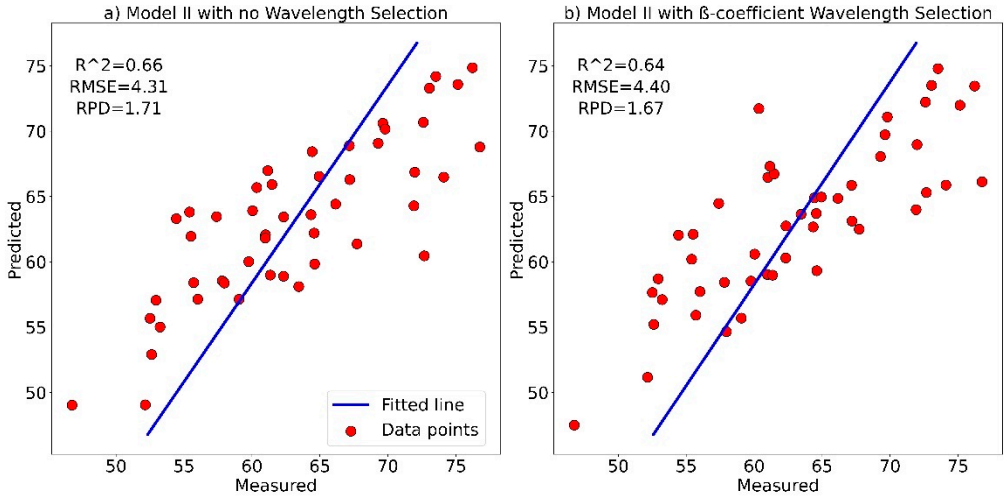


Figure 6. Measured vs. predicted moisture content in the case of selected optimum wavelengths using PLSR regression.

Onwude et al. [61] applied the combination of computer vision and backscattering imaging for predicting the moisture content and color changes of sweet potato. The RGB parameters and backscattering parameters were used in the study. It is observed that the calibration (R^2 = 0.66 and RMSEC = 0.19) and validation (R^2 = 0.63 and RMSEC = 0.19) model based on RGB parameters for predicting moisture content shows equal performance with our model II (choosing optimum wavelength). In fact, our model II performed well when compared with the calibration (R^2 = 0.59 and RMSEC = 0.20) and validation (R^2 = 0.54 and RMSEC = 0.22) model based on backscattering parameters for predicting moisture content.

This study aimed to determine the optimum wavelength range and preprocessing methods to predict moisture content in intact, unpeeled potatoes. The use of different varieties of potatoes in our study may have had some impact on the results obtained. It was noted that the spectral responses differed because of the different characteristics obtained from the various types of potatoes (data not shown). Nevertheless, the results presented here establish that hyperspectral imagery and PSLR regression can be used to provide an estimation of moisture content in potatoes. However, this is a preliminary study, and further

investigation is needed to improve the model quality. One important observation was that the predictive ability of the model was increased when using wavelengths between 733 and 970 nm, rather than the entire wavelength (400–1000 nm). This suggests that future work could focus on this wavelength range, potentially reducing the need for more expensive HSI sensors which can cover a wider spectral range. This study aims to investigate the feasibility of HSI in measuring the moisture content of unpeeled potatoes for determining the type of sensor. Thus, we could execute this method utilizing remotely sensed data by focusing on the moisture-specific bands identified in this study.

4. Conclusions

This paper investigated the feasibility of HSI to quantify the moisture content of unpeeled potatoes before they were subsequently stored and processed. Hyperspectral images were collected from 47 intact potato tubers, with partial least squares regression (PLSR) models developed to predict moisture content from these spectra. The models showed predictive abilities for moisture content, with acceptable ratios of prediction to deviation (RPDs) when considering the complete wavelength range (R^2 = 0.53; RPD = 1.46, root mean square error (RMSE) = 5.04%) or the β-coefficient wavelength selection technique (R^2 = 0.53; RPD = 1.47, RMSE = 5.02%). Furthermore, the prediction ability increased by more than 10% when the model wavelength was narrowed down to 733–970 nm. This study demonstrates the potential of using HSI for the quality assessment of intact, unpeeled potatoes, although further work is required to improve the model quality and implement this approach using remote sensing imagery. There are several limitations of this study. This study utilized a very limited sample for modeling and we will include more samples for measuring the model performance in the future. We also intend to test different sizes and varieties of potatoes for predicting moisture content and make an effort to incorporate samples that are collected directly from cultivars. An extended study will be carried out to analyze the spatial spectrum while predicting the moisture content.

Author Contributions: For Conceptualization, P.M., N.H.S., J.J., N.I., S.W. and S.G.; methodology, P.M., N.H.S., J.J. and N.I.; software, P.M., N.H.S., J.J. and N.I.; validation, P.M., N.H.S., J.J., N.I., S.W. and S.G.; writing—original draft preparation, P.M., N.H.S., J.J. and N.I.; writing—review and editing, P.M., N.H.S., J.J., N.I., S.W. and S.G.; supervision, N.H.S., N.I., S.W. and S.G.; project administration, N.H.S., N.I, S.W. and S.G. All authors have read and agreed to the published version of the manuscript.

Funding: This research received no external funding.

Institutional Review Board Statement: Not applicable.

Informed Consent Statement: Not applicable.

Data Availability Statement: The MC and HSI data are available upon request from authors.

Conflicts of Interest: The authors declare no conflict of interest.

References

1. United Nations Economic Commission for Europe (U.N.E.C.). Food Loss and Waste—The Case of Seed Potato Certification. Available online: https://unece.org/fileadmin/DAM/trade/agr/meetings/ge.06/2017/RapporteursMtg_TheNetherlands/Food_Loss_Waste.pdf (accessed on 10 November 2022).
2. Jennings, S.A.; Koehler, A.K.; Nicklin, K.J.; Deva, C.; Sait, S.M.; Challinor, A.J. Global potato yields increase under climate change with adaptation and CO_2 fertilisation. *Front. Sustain. Food Syst.* **2020**, *4*, 519324. [CrossRef]
3. FAO. International Year of the Potato. Available online: https://www.fao.org/agriculture/crops/thematic-sitemap/theme/hort-indust-crops/international-year-of-the-potato/en/ (accessed on 10 November 2022).
4. Amjad, W.; Crichton, S.O.; Munir, A.; Hensel, O.; Sturm, B. Hyperspectral imaging for the determination of potato slice moisture content and chromaticity during the convective hot air drying process. *Biosyst. Eng.* **2018**, *166*, 170–183. [CrossRef]
5. Amjad, W.; Hensel, O.; Munir, A. Batch drying of potato slices: Kinetic changes of colour and shrinkage in response of uniformly distributed drying temperature. *Agric. Eng. Int. CIGR J.* **2015**, *17*, 296–308.
6. Onu, C.E.; Igbokwe, P.K.; Nwabanne, J.T.; Nwajinka, C.O.; Ohale, P.E. Evaluation of optimization techniques in predicting optimum moisture content reduction in drying potato slices. *Artif. Intell. Agric.* **2020**, *4*, 39–47. [CrossRef]

7. Dong, J.; Guo, W. Nondestructive determination of apple internal qualities using near-infrared hyperspectral reflectance imaging. *Food Anal. Methods* **2015**, *8*, 2635–2646. [CrossRef]
8. Wu, D.; Sun, D.W. Advanced applications of hyperspectral imaging technology for food quality and safety analysis and assessment: A review—Part II: Applications. *Innov. Food Sci. Emerg. Technol.* **2013**, *19*, 15–28. [CrossRef]
9. Wu, D.; Shi, H.; Wang, S.; He, Y.; Bao, Y.; Liu, K. Rapid prediction of moisture content of dehydrated prawns using online hyperspectral imaging system. *Anal. Chim. Acta* **2012**, *726*, 57–66. [CrossRef]
10. Liu, D.; Qu, J.; Sun, D.-W.; Pu, H.; Zeng, X.A. Non-destructive prediction of salt contents and water activity of porcine meat slices by hyperspectral imaging in a salting process. *Innov. Food Sci. Emerg. Technol.* **2013**, *20*, 316–323. [CrossRef]
11. Murugan antham, P.; Wibowo, S.; Grandhi, S.; Samrat, N.H.; Islam, N. A systematic literature review on crop yield prediction with deep learning and remote sensing. *Remote Sens.* **2022**, *14*, 1990. [CrossRef]
12. Islam, N.; Rashid, M.; Wibowo, S.; Wasimi, S.; Morshed, A.; Xu, C.; Moore, S. Machine learning based approach for weed detection in chilli field using RGB images. In *Advances in Natural Computation, Fuzzy Systems and Knowledge Discovery*; Meng, H., Lei, T., Li, M., Li, K., Xiong, N., Wang, L., Eds.; Springer: Cham, Switzerland, 2021; Volume 88, pp. 1097–1105.
13. Islam, N.; Rashid, M.; Wibowo, S.; Xu, C.; Morshed, A.; Wasimi, S.; Moore, S.; Rahman, S.M. Early weed detection using image processing and machine learning techniques in an Australian chilli farm. *Agriculture* **2021**, *11*, 387. [CrossRef]
14. Adão, T.; Hruška, J.; Pádua, L.; Bessa, J.; Peres, E.; Morais, R.; Sousa, J.J. Hyperspectral imaging: A review on UAV-Based sensors, data processing and applications for agriculture and forestry. *Remote Sens.* **2017**, *9*, 1110. [CrossRef]
15. Tahmasbian, I.; Morgan, N.; Hosseini Bai, S.; Dunlop, M.; Moss, A. comparison of hyperspectral imaging and Near-Infrared spectroscopy to determine nitrogen and carbon concentrations in wheat. *Remote Sens.* **2021**, *13*, 1128. [CrossRef]
16. Mozgeris, G.; Jonikavičius, D.; Jovarauskas, D.; Zinkevičius, R.; Petkevičius, S.; Steponavičius, D. Imaging from manned ultra-light and unmanned aerial vehicles for estimating properties of spring wheat. *Precis. Agric.* **2018**, *19*, 876–894. [CrossRef]
17. Aasen, H.; Burkart, A.; Bolten, A.; Bareth, G. Generating 3D hyperspectral information with lightweight UAV snapshot cameras for vegetation monitoring: From camera calibration to quality assurance. *ISPRS J. Photogramm. Remote Sens.* **2015**, *108*, 245–259. [CrossRef]
18. Liu, H.; Bruning, B.; Garnett, T.; Berger, B. Hyperspectral imaging and 3D technologies for plant phenotyping: From satellite to close-range sensing. *Comput. Electron. Agric.* **2020**, *175*, 105621. [CrossRef]
19. Rajkumar, P.; Wang, N.; EImasry, G.; Raghavan, G.; Gariepy, Y. Studies on banana fruit quality and maturity stages using hyperspectral imaging. *J. Food Eng.* **2012**, *108*, 194–200. [CrossRef]
20. Schulz, H.; Drews, H.-H.; Quilitzsch, R.; Krüger, H. Application of near infrared spectroscopy for the quantification of quality parameters in selected vegetables and essential oil plants. *J. Near Infrared Spectrosc.* **1998**, *6*, A125–A130. [CrossRef]
21. Tarkosova, J.; Copikova, J. Determination of carbohydrate content in bananas during ripening and storage by near infrared spectroscopy. *J. Near Infrared Spectrosc.* **2000**, *8*, 21–26. [CrossRef]
22. Jin, H.; Li, L.; Cheng, J. Rapid and non-destructive determination of moisture content of peanut kernels using hyperspectral imaging technique. *Food Anal. Methods* **2015**, *8*, 2524–2532. [CrossRef]
23. Elbatawi, I.; Ebaid, M.; Hemeda, B. Determination of potato water content using nir diffuse reflection method. *Misr J. Agric. Eng.* **2008**, *25*, 1279–1292. [CrossRef]
24. Kjær, A.; Nielsen, G.; Stærke, S.; Clausen, M.R.; Edelenbos, M.; Jørgensen, B. Prediction of starch, soluble sugars and amino acids in potatoes (*Solanum tuberosum* L.) using hyperspectral imaging, dielectric and LF-NMR methodologies. *Potato Res.* **2016**, *59*, 357–374. [CrossRef]
25. Wang, F.; Wang, C.; Song, S.; Xie, S.; Kang, F. Study on starch content detection and visualization of potato based on hyperspectral imaging. *Food Sci. Nutr.* **2021**, *9*, 4420–4430. [CrossRef] [PubMed]
26. Rady, A.; Guyer, D.; Lu, R. Evaluation of sugar content of potatoes using hyperspectral imaging. *Food Bioprocess Technol.* **2015**, *8*, 995–1010. [CrossRef]
27. Li, B.; Xu, X.; Zhang, L.; Han, J.; Bian, C.; Li, G.; Liu, J.; Jin, L. Above-ground biomass estimation and yield prediction in potato by using UAV-based RGB and hyperspectral imaging. *ISPRS J. Photogramm. Remote Sens.* **2020**, *162*, 161–172. [CrossRef]
28. Nigon, T.; Rosen, C.; Mulla, D.; Cohen, Y.; Alchanatis, V.; Rud, R. Hyperspectral imagery for the detection of nitrogen stress in potato for in-season management. In Proceedings of the 11th International Conference on Precision Agriculture, [CD-ROM], Indianapolis, IN, USA, 15–18 July 2012.
29. López-Maestresalas, A.; Keresztes, J.C.; Goodarzi, M.; Arazuri, S.; Jarén, C.; Saeys, W. Non-destructive detection of blackspot in potatoes by Vis-NIR and SWIR hyperspectral imaging. *Food Control* **2016**, *70*, 229–241. [CrossRef]
30. Ye, D.; Sun, L.; Tan, W.; Che, W.; Yang, M. Detecting and classifying minor bruised potato based on hyperspectral imaging. *Chemom. Intell. Lab. Syst.* **2018**, *177*, 129–139. [CrossRef]
31. Gao, Y.; Li, Q.; Rao, X.; Ying, Y. Precautionary analysis of sprouting potato eyes using hyperspectral imaging technology. *Int. J. Agric. Biol. Eng.* **2018**, *11*, 153–157. [CrossRef]
32. Shao, Y.; Liu, Y.; Xuan, G.; Wang, Y.; Gao, Z.; Hu, Z.; Han, X.; Gao, C.; Wang, K. Application of hyperspectral imaging for spatial prediction of soluble solid content in sweet potato. *RSC Adv.* **2020**, *10*, 33148–33154. [CrossRef]
33. Do Trong, N.N.; Tsuta, M.; Nicolaï, B.; De Baerdemaeker, J.; Saeys, W. Prediction of optimal cooking time for boiled potatoes by hyperspectral imaging. *J. Food Eng.* **2011**, *105*, 617–624. [CrossRef]

34. Duarte-Carvajalino, J.M.; Silva-Arero, E.A.; Góez-Vinasco, G.A.; Torres-Delgado, L.M.; Ocampo-Paez, O.D.; Castaño-Marín, A.M. Estimation of water stress in potato plants using hyperspectral imagery and machine learning algorithms. *Horticulturae* **2021**, *7*, 176. [CrossRef]
35. Sun, Y.; Liu, Y.; Yu, H.; Xie, A.; Li, X.; Yin, Y.; Duan, X. Non-destructive prediction of moisture content and freezable water content of purple-fleshed sweet potato slices during drying process using hyperspectral imaging technique. *Food Anal. Methods* **2017**, *10*, 1535–1546. [CrossRef]
36. Xiao, Q.; Bai, X.; He, Y. Rapid screen of the color and water content of fresh-cut potato tuber slices using hyperspectral imaging coupled with multivariate analysis. *Foods* **2020**, *9*, 94. [CrossRef] [PubMed]
37. Bouraoui, M.; Richard, P.; Fichtali, J. A review of moisture content determination in foods using microwave oven drying. *Food Res. Int.* **1993**, *26*, 49–57. [CrossRef]
38. Pu, Y.-Y.; Sun, D.-W. Vis–NIR hyperspectral imaging in visualizing moisture distribution of mango slices during microwave-vacuum drying. *Food Chem.* **2015**, *188*, 271–278. [CrossRef]
39. Jung, A.; Vohland, M.; Thiele-Bruhn, S. Use of a portable camera for proximal soil sensing with hyperspectral image data. *Remote Sens.* **2015**, *7*, 11434–11448. [CrossRef]
40. Buddenbaum, H.; Steffens, M. The effects of spectral pretreatments on chemometric analyses of soil profiles using laboratory imaging spectroscopy. *Appl. Environ. Soil Sci.* **2012**, *2012*, 274903. [CrossRef]
41. Yan, H.; Li, P.-H.; Zhou, G.-S.; Wang, Y.-J.; Bao, B.-H.; Wu, Q.-N.; Huang, S.-L. Rapid and practical qualitative and quantitative evaluation of non-fumigated ginger and sulfur-fumigated ginger via Fourier-transform infrared spectroscopy and chemometric methods. *Food Chem.* **2021**, *341*, 128241. [CrossRef]
42. Samrat, N.H.; Johnson, J.B.; White, S.; Naiker, M.; Brown, P. A Rapid Non-Destructive Hyperspectral Imaging Data Model for the Prediction of Pungent Constituents in Dried Ginger. *Foods* **2022**, *11*, 649. [CrossRef]
43. Sädekoski, N. Tropical Altitudinal Gradient Soil Organic Carbon Estimation with VIS-NIR (400–1000 nm) Imaging Spectroscopy. Master's Thesis, University of Helsinki, Helsinki, Finland, 2020.
44. Vasques, G.; Grunwald, S.; Sickman, J. Comparison of multivariate methods for inferential modeling of soil carbon using visible/near-infrared spectra. *Geoderma* **2008**, *146*, 14–25. [CrossRef]
45. Kämper, W.; Trueman, S.J.; Tahmasbian, I.; Bai, S.H. Rapid determination of nutrient concentrations in Hass avocado fruit by Vis/NIR hyperspectral imaging of flesh or skin. *Remote Sens.* **2020**, *12*, 3409. [CrossRef]
46. Lin, X.; Sun, D.-W. Investigation of moisture distribution of ginger slices and splits during hot-air drying and rehydration procedures by NIR hyperspectral imaging. In Proceedings of the Sensing for Agriculture and Food Quality and Safety XII, Online, 27 April–1 May 2020; p. 114210D.
47. Rossel, R.V.; Walvoort, D.; McBratney, A.; Janik, L.J.; Skjemstad, J. Visible, near infrared, mid infrared or combined diffuse reflectance spectroscopy for simultaneous assessment of various soil properties. *Geoderma* **2006**, *131*, 59–75. [CrossRef]
48. Malmir, M.; Tahmasbian, I.; Xu, Z.; Farrar, M.B.; Bai, S.H. Prediction of soil macro-and micro-elements in sieved and ground air-dried soils using laboratory-based hyperspectral imaging technique. *Geoderma* **2019**, *340*, 70–80. [CrossRef]
49. Rodríguez-Pulido, F.J.; Gordillo, B.; Heredia, F.J.; González-Miret, M.L. CIELAB–Spectral image MATCHING: An app for merging colorimetric and spectral images for grapes and derivatives. *Food Control* **2021**, *125*, 108038. [CrossRef]
50. Abdi, H. Partial least squares regression and projection on latent structure regression (PLS Regression). *WIREs Comput. Stat.* **2010**, *2*, 97–106. [CrossRef]
51. Malmir, M.; Tahmasbian, I.; Xu, Z.; Farrar, M.B.; Bai, S.H. Prediction of macronutrients in plant leaves using chemometric analysis and wavelength selection. *J. Soils Sediments* **2020**, *20*, 249–259. [CrossRef]
52. Liu, Y.; Lyu, Q.; He, S.; Yi, S.; Liu, X.; Xie, R.; Zheng, Y.; Deng, L. Prediction of nitrogen and phosphorus contents in citrus leaves based on hyperspectral imaging. *Int. J. Agric. Biol. Eng.* **2015**, *8*, 80–88.
53. Hossin, M.; Sulaiman, M. A review on evaluation metrics for data classification evaluations. *Int. J. Data Min. Knowl. Manag. Process* **2015**, *5*, 1.
54. Su, W.H.; Xue, H. Imaging spectroscopy and machine learning for intelligent determination of potato and sweet potato quality. *Foods* **2021**, *10*, 2146. [CrossRef]
55. Zhu, H.; Chu, B.; Fan, Y.; Tao, X.; Yin, W.; He, Y. Hyperspectral imaging for predicting the internal quality of Kiwifruits based on variable selection algorithms and chemometric models. *Sci. Rep.* **2017**, *7*, 7845. [CrossRef]
56. Iqbal, A.; Sun, D.-W.; Allen, P. Prediction of moisture, color and pH in cooked, pre-sliced turkey hams by NIR hyperspectral imaging system. *J. Food Eng.* **2013**, *117*, 42–51. [CrossRef]
57. John, R.; Bhardwaj, R.; Jeyaseelan, C.; Bollinedi, H.; Singh, N.; Harish, G.; Singh, R.; Nath, D.J.; Arya, M.; Sharma, D. Germplasm variability-assisted near infrared reflectance spectroscopy chemometrics to develop multi-trait robust prediction models in rice. *Front. Nutr.* **2022**, *2022*, 946255. [CrossRef] [PubMed]
58. Mehmood, T.; Liland, K.H.; Snipen, L.; Sæbø, S. A review of variable selection methods in Partial Least Squares Regression. *Chemom. Intell. Lab. Syst.* **2012**, *118*, 62–69. [CrossRef]
59. Xu, S.; Zhao, Y.; Wang, M.; Shi, X. Comparison of multivariate methods for estimating selected soil properties from intact soil cores of paddy fields by Vis–NIR spectroscopy. *Geoderma* **2018**, *310*, 29–43. [CrossRef]

60. Ruett, M.; Junker-Frohn, L.V.; Siegmann, B.; Ellenberger, J.; Jaenicke, H.; Whitney, C.; Luedeling, E.; Tiede-Arlt, P.; Rascher, U. Hyperspectral imaging for high-throughput vitality monitoring in ornamental plant production. *Sci. Hortic.* **2022**, *291*, 110546. [CrossRef]
61. Onwude, D.I.; Hashim, N.; Abdan, K.; Janius, R.; Chen, G. Combination of computer vision and backscattering imaging for predicting the moisture content and colour changes of sweet potato (*Ipomoea batatas* L.) during drying. *Comput. Electron. Agric.* **2018**, *150*, 178–187. [CrossRef]

Disclaimer/Publisher's Note: The statements, opinions and data contained in all publications are solely those of the individual author(s) and contributor(s) and not of MDPI and/or the editor(s). MDPI and/or the editor(s) disclaim responsibility for any injury to people or property resulting from any ideas, methods, instructions or products referred to in the content.